Hindawi
Advances in Mathematical Physics
Volume 2020, Article ID 5849690, 13 pages
https://doi.org/10.1155/2020/5849690

Research Article

Heat Concentration around a Cylindrical Interface Crack in a Composite Tube

J. W. Fu [1] and L. F. Qian [1,2]

[1]*Department of Mechanical Engineering, Nanjing University of Science and Technology, Nanjing, Jiangsu 210094, China*
[2]*Northwest Institute of Mechanical and Electrical Engineering, Xianyang, Shaanxi 712099, China*

Correspondence should be addressed to L. F. Qian; lfqian@njust.edu.cn

Received 10 April 2020; Accepted 2 May 2020; Published 12 June 2020

Academic Editor: Marin Marin

Cracks always form at the interface of discrepant materials in composite structures, which influence thermal performances of the structures under transient thermal loadings remarkably. The heat concentration around a cylindrical interface crack in a bilayered composite tube has not been resolved in literature and thus is investigated in this paper based on the singular integral equation method. The time variable in the two-dimensional temperature governing equation, derived from the non-Fourier theory, is eliminated using the Laplace transformation technique and then solved exactly in the Laplacian domain by the employment of a superposition method. The heat concentration degree caused by the interface crack is judged quantitatively with the employment of heat flux intensity factor. After restoring the results in the time domain using a numerical Laplace inversion technique, the effects of thermal resistance of crack, liner material, and crack length on the results are analyzed with a numerical case study. It is found that heat flux intensity factor is material-dependent, and steel is the best liner material among the three potential materials used for sustaining transiently high temperature loadings.

1. Introduction

As a kind of star material, fiber reinforced resin matrix (FRRM) composite tubes with adhesive layers have been extensively used in weight-sensitive engineering applications, such as automobile, aircrafts, and gun tube. FRRM composites are used to reduce the weight of a structure, while the adhesive layer can usually protect the structure from the severely thermal and mechanical loadings. However, due to the manufacturing issue and the discrepancy of material properties between the FRRM composite and adhesive layer, their interface will sometimes debond and form an interface crack which affects the structure performance remarkably. The continuity of the heat flow in the structure under transient thermal loadings is destroyed by the crack, which causes heat concentration around the crack tip. Various aspects of composite structures have been studied, such as the constitutive equations of composite structures [1], the thermoelastic responses under transient thermal loadings [2], and the way to enhance the rigidity of composite plates [3].

Back in 1965, Sih [4] studied the thermal disturbance problem in an infinite region with lines of crack by adopting the complex variable method and found that heat flux processed the inverse square root singularity around the crack tip. Tzou [5] confirmed the singularity behavior by introducing the intensity factor of a temperature gradient. Heat conduction of plates containing multiple insulated cracks under arbitrary Neumann thermal conditions was investigated by Chen and Chang [6]. As to the interface crack, Chao and Chang [7] obtained the exact temperature solutions for a composite media made of dissimilar anisotropic materials with a crack located at the interface. The similar problem with the consideration of interstitial medium filled between dissimilar anisotropic materials was investigated by Shiah and Shi [8]. Chiu et al. [9] calculated the temperature distribution in an infinitely functionally graded (FG) plane containing an arbitrarily oriented crack. Zhou et al. [10] considered a partially insulated interface crack of a homogeneous orthotropic substrate coated by a graded orthotropic layer. And, an interface crack in a bilayered magnetoelectroelastic

material under heat flow loadings was analyzed by Gao and Noda [11]. Wang et al. [12] discussed the effect of thermal resistance of a cohesive zone on the thermal fracture of mode II crack under static thermal loadings.

Recently, non-Fourier heat conduction theories have found their applications on the thermal study of cracked structures. These new theories were created to eliminate the drawback of the classical Fourier one that the thermal wave propagates at an infinitely large speed. Among these theories, the heat conduction model proposed by Cattaneo [13] and Vernotte [14] (C-V model) has experimentally proved that this model could accurately predict the finite thermal propagation speed in processed meat and some materials with non-homogeneous inner structures [15, 16]. Some other non-Fourier heat conduction models including the commonly used dual-phase-lag (DPL) model were reviewed in Ref. [17]. The generalized thermoelastic theory, extended from the C-V model, has been used to study the thermomechanical coupling effects under various loading conditions, such as pulsed laser heating [18]. Chen and Hu [19] got the disturbed temperature field of an infinite half-plane coated by a thin layer containing an insulated interface crack using the C-V model, while the DPL model was used to conduct the crack problem in a half-plane by Hu and Chen [20]. The transient non-Fourier temperature and corresponding thermoelastic fields of a half-plane [21] or strip [22] with a crack parallel to the surface subjected to thermal shock were investigated using the singular integral equation method. Xue et al. [23] revisited the thermoelastic problem of a crack in a strip based on the memory-dependent heat conduction model. Fu et al. [24] conducted the thermal analysis of a sandwich structure with a cracked foam core based on the non-Fourier heat conduction model. Cracks lead to a kind of mathematical problem termed as mixed-boundary-value problem; another similar mathematical problem termed as mixed-initial-boundary-value problem can be found in [25–27], in which thermoelastic responses of micropolar porous bodies are considered.

As to cylindrical structures, Guo et al. [28] obtained the temperature field and stress intensity factor (SIF) for a penny-shaped crack using the DPL heat conduction theory. An insulated penny-shaped crack in an elastic half-space was handled by employing the fractional-order non-Fourier heat conduction model [29]. The transient thermoelastic fields of isotropic or transversely isotropic cylinders containing a circumferential crack were investigated based on different kinds of non-Fourier models, and the corresponding thermal SIFs were calculated therein [30–34]. It should be noted that the circumferential crack, spreading along the radial direction, did not disturb the temperature field as the temperature loading was applied on the lateral surfaces.

On the contrary, the cylindrical crack spreading along the axial direction would disturb the heat flow in the radial direction remarkably. However, the investigation on cylindrical cracks among most of the works published to date is limited to mechanical loading conditions such as tension and torsion [35–39], and the work on its thermal analysis is rare. The thermoelastic study of cylindrical cracks under static thermal loadings was conducted by Itou [40]. Recently, Fu et al. [41] analyzed the disturbed temperature field of a FG cylinder containing a cylindrical crack.

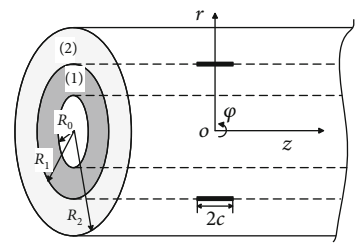

Figure 1: A composite tube with a cylindrical interface crack.

To the authors' knowledge, the heat conduction in the composite tubes affected by the cylindrical interface crack has not been resolved even using the classical Fourier theory. The current work is designed to study the heat concentration behavior of a cracked bilayered composite tube with the adoption of non-Fourier heat conduction theory. The C-V heat conduction model and the problem with corresponding boundary conditions are described in Section 2, and the solution procedure based on the singular integral equation is illustrated in Section 3 in detail. Section 4 gives the expressions of temperature field and heat flux intensity factor (HFIF). Moreover, the effects of crack face resistance, liner material, and crack length are analyzed in Section 5. Finally, the main conclusions of this paper are summarized in Section 6.

2. Problem Formulation

A bilayered composite tube with an inner radius R_0 and outer radius R_2 is located in the cylindrical coordinate $O - r\varphi z$, as illustrated in Figure 1. The sudden change of external and internal environments of the tube will lead to a dynamic heat flow in the structure, which could be disturbed remarkably by the cylindrical crack occupying the region $-c < z < c$ at the interface $r = R_1$. The tube with uniform initial temperature T_0 is assumed infinitely long and will not deform under thermal loadings. The outer layer (2) is the fiber reinforced resin matrix composite with fibers parallel to the axis and randomly distributed in the resin, while the material of the inner layer (1) is a thermal protective liner and has significantly higher strength.

The heat flux in the radial and axial directions within the C-V model takes the form.

$$\begin{gathered}\left(1+\tau^{(i)}\frac{\partial}{\partial t}\right)q_r^{(i)}(r,z,t) = -\lambda_r^{(i)}\frac{\partial T^{(i)}(r,z,t)}{\partial r},\\ \left(1+\tau^{(i)}\frac{\partial}{\partial t}\right)q_z^{(i)}(r,z,t) = -\lambda_z^{(i)}\frac{\partial T^{(i)}(r,z,t)}{\partial z},\\ i = 1, 2,\end{gathered} \tag{1}$$

in which, q_r and q_z are the heat flux in the radial and axial direction, respectively, t is the time, and T is the temperature. λ_r and λ_z are, respectively, the thermal conductivity in the transverse plane and longitudinal direction for the

transversely isotropic composite layer, and $\lambda_r = \lambda_z$ holds for the isotropic inner layer. Please note that the thermal properties of fiber reinforced composite material will take its macroscopically equivalent parameters. The phase lag of heat flux τ, which can be interpreted as the time lag needed to excite heat flow at a position when a temperature gradient loading is applied on that position, is an intrinsic material property with the unit of time and varies from 10^{-14}~10^{2} s for different materials. It can be easily seen from Equation (1) that $\tau = 0$ reduces the C-V model to the Fourier one.

Without considering the heat source, the energy conservation equation reads

$$-\left(\frac{\partial q_r^{(i)}}{\partial r} + \frac{q_r^{(i)}}{r} + \frac{\partial q_z^{(i)}}{\partial z}\right) = \rho^{(i)} c_P^{(i)} \frac{\partial T^{(i)}}{\partial t}, \tag{2}$$

where c_P and ρ are specific heat capacity and mass density, respectively.

The temperature governing equation can be obtained by eliminating the heat flux from Equation (2) and Equation (1) as

$$\left(1 + \tau^{(i)} \frac{\partial}{\partial t}\right) \frac{\partial T^{(i)}}{\partial t} = \left[d_r^{(i)} \left(\frac{\partial^2}{\partial r^2} + \frac{\partial}{r \partial r}\right) + d_z^{(i)} \frac{\partial^2}{\partial z^2}\right] T^{(i)}, \quad i = 1, 2, \tag{3}$$

where $d = \lambda / \rho c_P$ is the thermal diffusivity. Equation (3) also indicates that the speed of thermal wave in the radial direction is $C_{\mathrm{CV}} = \sqrt{d_r / \tau}$.

The thermal boundary conditions for the cracked tube can be written as

$$q_r^{(1)}(R_0, z, t) = -h_i \left[T^{(1)}(R_0, z, t) - T_a(t)\right], \quad |z| < \infty, \tag{4}$$

$$q_r^{(2)}(R_2, z, t) = h_o \left[T^{(2)}(R_2, z, t) - T_b(t)\right], \quad |z| < \infty, \tag{5}$$

$$q_r^{(1)}(R_1, z, t) = q_r^{(2)}(R_1, z, t), \quad |z| < \infty, \tag{6}$$

$$T^{(1)}(R_1, z, t) = T^{(2)}(R_1, z, t), \quad |z| \geq c, \tag{7}$$

$$V q_r^{(1)}(R_1, z, t) = T^{(1)}(R_1, z, t) - T^{(2)}(R_1, z, t), \quad |z| < c. \tag{8}$$

The convective heat transfer conditions between surfaces of the tube and its corresponding environments with temperature T_a and T_b are shown in Equations (4) and (5), where h_i and h_o are heat transfer coefficients. Equations (6) and (7) describe the thermal conditions at the interface. It can be easily seen that the mixed boundary condition, given by Equations (7) and (8), brings much mathematical complexity. It should be noted that a zero value of thermal resistance V represents a perfectly conductive crack, while an insulated crack generates for an infinitely large value of V.

3. Solution of the Mixed-Boundary-Condition Problem

In this section, the Laplace transform and Fourier transform as well as the superposition method are adopted to solve the problem. It should be mentioned that the singular integral equation method is originally proposed by Erdogan et al. [42] to study the mechanical fracture problems, and this paper extends the method to investigate the mixed-boundary-condition problem in thermal fields. The mismatch of thermal properties of the material on the sides of crack improves the mathematical complexity and leads to a material-property-dependent HFIF.

In order to normalize the equations, the following nondimensional parameters are introduced:

$$\begin{aligned} t' &= \frac{t d^{(0)}}{c^2}, \\ \tau^{(i)\prime} &= \frac{\tau^{(i)} d^{(0)}}{c^2}, \\ r' &= \frac{r}{c}, \\ h_i' &= \frac{h_i c}{\lambda^{(0)}}, \\ T^{(i)\prime} &= \frac{T^{(i)} - T_0}{T_0}, \\ V' &= \frac{V \lambda^{(0)}}{c}, \\ q^{(i)\prime} &= \frac{q^{(i)} c}{\lambda^{(0)} T_0}. \end{aligned} \tag{9}$$

It should be mentioned that other dimensional parameters with the same unit as those in Equation (9) could be normalized accordingly. The parameters with the superscript "0" are reference properties.

Substituting the nondimensional parameters in Equation (9) into Equation (3), the governing equation can be rewritten as

$$\left(\frac{\partial^2}{\partial r'^2} + \frac{1}{r'} \frac{\partial}{\partial r'} + \upsilon^{(i)2} \frac{\partial^2}{\partial z'^2}\right) T^{(i)\prime} = \frac{d^{(0)}}{d_r^{(i)}} \left(1 + \tau^{(i)\prime} \frac{\partial}{\partial t'}\right) \frac{\partial T^{(i)\prime}}{\partial t'}, \tag{10}$$

where $\upsilon^{(i)2} = d_z^{(i)} / d_r^{(i)}$. When zero initial temperature change and rate of temperature change are assumed, Laplace transformation is applied to Equation (10) to eliminate the time variable t', as

$$\left(\frac{\partial^2}{\partial r'^2} + \frac{1}{r'} \frac{\partial}{\partial r'} + \upsilon^{(i)2} \frac{\partial^2}{\partial z'^2}\right) \tilde{T}^{(i)\prime} - k_1^{(i)} \tilde{T}^{(i)\prime} = 0, \tag{11}$$

in which, $k_1^{(i)} = s(1 + \tau^{(i)\prime} s) d^{(0)} / d_r^{(i)}$ and s is the Laplace variable.

Equations (4)–(8) are treated with similar nondimensionalization and Laplace transformation operations, and the boundary conditions are rewritten as

$$\tilde{q}_r^{(1)\prime}\left(R_0', z', s\right) = -h_i'\left[\tilde{T}^{(1)'}\left(R_0', z', s\right) - \tilde{T}_a'(s)\right], \tag{12}$$

$$\tilde{q}_r^{(2)\prime}\left(R_2', z', s\right) = h_o'\left[\tilde{T}^{(2)'}\left(R_2', z', s\right) - \tilde{T}_b'(s)\right], \tag{13}$$

$$\tilde{q}_r^{(1)\prime}\left(R_1', z', s\right) = \tilde{q}_r^{(2)\prime}\left(R_1', z', s\right), \tag{14}$$

$$\tilde{T}^{(1)'}\left(R_1', z', s\right) = \tilde{T}^{(2)'}\left(R_1', z', s\right), \quad \left|z'\right| \geq 1, \tag{15}$$

$$V'\tilde{q}_r^{(1)\prime}\left(R_1', z', s\right) = \tilde{T}^{(1)'}\left(R_1', z', s\right) - \tilde{T}^{(2)'}\left(R_1', z', s\right), \quad \left|z'\right| < 1. \tag{16}$$

The governing equation (11) under the boundaries (12)–(16) can be solved using the superposition method. The first problem (P1) can be described as inner and outer surfaces of an uncracked tube applied with inhomogeneous boundary conditions. And the second problem (P2) is a cracked tube without thermal loadings applied on the surfaces. The mathematical expressions of P1 and P2 are, respectively, as follows:

P1:

$$\begin{aligned}
&\left(\frac{d^2}{dr'^2} + \frac{1}{r'}\frac{d}{dr'}\right)\tilde{T}_1^{(i)\prime} - k_1^{(i)}\tilde{T}_1^{(i)\prime} = 0,\\
&\tilde{q}_{r1}^{(1)\prime}\left(R_0', s\right) = -h_i'\left[\tilde{T}_1^{(1)\prime}\left(R_0', s\right) - \tilde{T}'_a(s)\right],\\
&\tilde{q}_{r1}^{(2)\prime}\left(R_2', s\right) = h_o'\left[\tilde{T}_1^{(2)\prime}\left(R_2', s\right) - \tilde{T}'_b(s)\right],\\
&\tilde{q}_{r1}^{(1)\prime}\left(R_1', s\right) = \tilde{q}_{r1}^{(2)\prime}\left(R_1', s\right),\\
&\tilde{T}_1^{(1)\prime}\left(R_1', s\right) = \tilde{T}_1^{(2)\prime}\left(R_1', s\right),
\end{aligned} \tag{17}$$

P2:

$$\left(\frac{\partial^2}{\partial r'^2} + \frac{1}{r'}\frac{\partial}{\partial r'} + \upsilon^{(i)2}\frac{\partial^2}{\partial z'^2}\right)\tilde{T}_2^{(i)\prime} - k_1^{(i)}\tilde{T}_2^{(i)\prime} = 0, \tag{18}$$

$$\tilde{q}_{r2}^{(1)\prime}\left(R_0', z', s\right) = -h_i'\tilde{T}_2^{(1)\prime}\left(R_0', z', s\right), \tag{19}$$

$$\tilde{q}_{r2}^{(2)\prime}\left(R_2', z', s\right) = h_o'\tilde{T}_2^{(2)\prime}\left(R_2', z', s\right), \tag{20}$$

$$\tilde{q}_{r2}^{(1)\prime}\left(R_1', z', s\right) = \tilde{q}_{r2}^{(2)\prime}\left(R_1', z', s\right), \tag{21}$$

$$\tilde{T}_2^{(1)\prime}\left(R_1', z', s\right) = \tilde{T}_2^{(2)\prime}\left(R_1', z', s\right), \quad \left|z'\right| \geq 1, \tag{22}$$

$$\begin{aligned}
V'\left[\tilde{q}_{r1}^{(1)\prime}\left(R_1', s\right) + \tilde{q}_{r2}^{(1)\prime}\left(R_1', z', s\right)\right] &= \tilde{T}_2^{(1)\prime}\left(R_1', z', s\right)\\
&- \tilde{T}_2^{(2)\prime}\left(R_1', z', s\right), \quad \left|z'\right| < 1.
\end{aligned} \tag{23}$$

The actual results of temperature and heat flux are addition of the solution of P1 and P2 as $\tilde{T}^{(i)'} = \tilde{T}_1^{(i)\prime} + \tilde{T}_2^{(i)\prime}$ and $\tilde{q}_r^{(i)\prime} = \tilde{q}_{r1}^{(i)\prime} + \tilde{q}_{r2}^{(i)\prime}$.

The solution of P1 can be easily obtained as

$$\tilde{T}_1^{(i)\prime} = S_1^{(i)} I_0\left(\sqrt{k_1^{(i)}}r'\right) + S_2^{(i)} K_0\left(\sqrt{k_1^{(i)}}r'\right), \tag{24}$$

$$\tilde{q}_{r1}^{(i)\prime} = k_2^{(i)}\sqrt{k_1^{(i)}}\left[S_1^{(i)} I_1\left(\sqrt{k_1^{(i)}}r'\right) - S_2^{(i)} K_1\left(\sqrt{k_1^{(i)}}r'\right)\right], \tag{25}$$

where $k_2^{(i)} = -(\lambda^{(i)}/\lambda^{(0)})(1/(1+\tau^{(i)'}s))$ and $I_n()$ and $K_n()$ represent the nth-order modified Bessel functions of the first kind and the second, respectively. The unknowns $S_1^{(i)}$ and $S_2^{(i)}$ can be obtained from $\mathbf{PS} = \mathbf{Q}$, in which, $\mathbf{S}$ is defined as

$$\mathbf{S} = \left[S_1^{(1)} \;\; S_2^{(1)} \;\; S_1^{(2)} \;\; S_2^{(2)}\right]^{\mathrm{T}}, \tag{26}$$

and the nonzero elements of 4×4 matrix $\mathbf{P}$ and 4×1 vector $\mathbf{Q}$ are

$$\begin{aligned}
P_{1,1} &= k_2^{(1)}\sqrt{k_1^{(1)}} I_1\left(\sqrt{k_1^{(1)}}R_0'\right) + h_i' I_0\left(\sqrt{k_1^{(1)}}R_0'\right),\\
P_{1,2} &= -k_2^{(1)}\sqrt{k_1^{(1)}} K_1\left(\sqrt{k_1^{(1)}}R_0'\right) + h_i' K_0\left(\sqrt{k_1^{(1)}}R_0'\right),\\
P_{2,3} &= -k_2^{(2)}\sqrt{k_1^{(2)}} I_1\left(\sqrt{k_1^{(2)}}R_2'\right) + h_o' I_0\left(\sqrt{k_1^{(2)}}R_2'\right),\\
P_{2,4} &= k_2^{(2)}\sqrt{k_1^{(2)}} K_1\left(\sqrt{k_1^{(2)}}R_2'\right) + h_o' K_0\left(\sqrt{k_1^{(2)}}R_2'\right),\\
P_{3,1} &= k_2^{(1)}\sqrt{k_1^{(1)}} I_1\left(\sqrt{k_1^{(1)}}R_1'\right),\\
P_{3,2} &= -k_2^{(1)}\sqrt{k_1^{(1)}} K_1\left(\sqrt{k_1^{(1)}}R_1'\right),\\
P_{3,3} &= -k_2^{(2)}\sqrt{k_1^{(2)}} I_1\left(\sqrt{k_1^{(2)}}R_1'\right),\\
P_{3,4} &= k_2^{(2)}\sqrt{k_1^{(2)}} K_1\left(\sqrt{k_1^{(2)}}R_1'\right),\\
P_{4,1} &= -I_0\left(\sqrt{k_1^{(1)}}R_1'\right),\\
P_{4,2} &= -K_0\left(\sqrt{k_1^{(1)}}R_1'\right),\\
P_{4,3} &= I_0\left(\sqrt{k_1^{(2)}}R_1'\right),\\
P_{4,4} &= K_0\left(\sqrt{k_1^{(2)}}R_1'\right),\\
Q_1 &= h_i'\tilde{T}'_a(s),\\
Q_2 &= h_o'\tilde{T}'_b(s).
\end{aligned} \tag{27}$$

The application of the Fourier transformation,

$$\bar{f}(\xi) = \int_{-\infty}^{\infty} f\left(z'\right) e^{-j\xi z'} dz', \tag{28}$$

to Equation (18) leads to

$$\left(\frac{\partial^2}{\partial r'^2} + \frac{1}{r'}\frac{\partial}{\partial r'} - k_3^{(i)}\right) \bar{\tilde{T}}_2^{(i)\prime} = 0, \tag{29}$$

where $k_3^{(i)} = \upsilon^{(i)2}\xi^2 + k_1^{(i)}$ and ξ is the Fourier transformation variable. Thus, the temperature and heat flux in the double-transformed domain can be solved as

$$\begin{aligned}
\bar{\tilde{T}}_2^{(i)\prime} &= S_3^{(i)} I_0\left(\sqrt{k_3^{(i)}} r'\right) + S_4^{(i)} K_0\left(\sqrt{k_3^{(i)}} r'\right), \\
\bar{\tilde{q}}_2^{(i)\prime} &= k_2^{(i)} \sqrt{k_3^{(i)}} \left[S_3^{(i)} I_1\left(\sqrt{k_3^{(i)}} r'\right) - S_4^{(i)} K_1\left(\sqrt{k_3^{(i)}} r'\right)\right].
\end{aligned} \tag{30}$$

The corresponding temperature and the heat flux in the Laplace domain are then calculated using the Fourier inversion transform,

$$f\left(z'\right) = \frac{1}{2\pi}\int_{-\infty}^{\infty} \bar{f}(\xi) e^{j\xi z'} d\xi, \tag{31}$$

as

$$\tilde{T}_2^{(i)\prime} = \frac{1}{2\pi}\int_{-\infty}^{\infty} \left[S_3^{(i)} I_0\left(\sqrt{k_3^{(i)}} r'\right) + S_4^{(i)} K_0\left(\sqrt{k_3^{(i)}} r'\right)\right] e^{j\xi z'} d\xi, \tag{32}$$

$$\tilde{q}_2^{(i)\prime} = \frac{1}{2\pi}\int_{-\infty}^{\infty} k_2^{(i)} \sqrt{k_3^{(i)}} \left[S_3^{(i)} I_1\left(\sqrt{k_3^{(i)}} r'\right) - S_4^{(i)} K_1\left(\sqrt{k_3^{(i)}} r'\right)\right] e^{j\xi z'} d\xi, \tag{33}$$

where the imaginary number $j = \sqrt{-1}$.

Using the boundary equations (18)–(21), the unknowns in Equation (32) are linked as

$$\begin{aligned}
S_3^{(1)} &= -\frac{X_2 X_5}{X_1} S_4^{(2)}, \\
S_4^{(1)} &= X_5 S_4^{(2)}, \\
S_3^{(2)} &= -\frac{X_4}{X_3} S_4^{(2)},
\end{aligned} \tag{34}$$

in which

$$\begin{aligned}
X_1 &= h_i' I_0\left(\sqrt{k_3^{(1)}} R_0'\right) + k_2^{(1)} \sqrt{k_3^{(1)}} I_1\left(\sqrt{k_3^{(1)}} R_0'\right), \\
X_2 &= h_i' K_0\left(\sqrt{k_3^{(1)}} R_0'\right) - k_2^{(1)} \sqrt{k_3^{(1)}} K_1\left(\sqrt{k_3^{(1)}} R_0'\right), \\
X_3 &= h_o' I_0\left(\sqrt{k_3^{(2)}} R_2'\right) - k_2^{(2)} \sqrt{k_3^{(2)}} I_1\left(\sqrt{k_3^{(2)}} R_2'\right), \\
X_4 &= h_o' K_0\left(\sqrt{k_3^{(2)}} R_2'\right) + k_2^{(2)} \sqrt{k_3^{(2)}} K_1\left(\sqrt{k_3^{(2)}} R_2'\right), \\
X_5 &= \frac{k_2^{(2)} \sqrt{k_3^{(2)}} I_1\left(\sqrt{k_3^{(2)}} R_1'\right)(X_4/X_3) + k_2^{(2)} \sqrt{k_3^{(2)}} K_1\left(\sqrt{k_3^{(2)}} R_1'\right)}{k_2^{(1)} \sqrt{k_3^{(1)}} I_1\left(\sqrt{k_3^{(1)}} R_1'\right)(X_2/X_1) + k_2^{(1)} \sqrt{k_3^{(1)}} K_1\left(\sqrt{k_3^{(1)}} R_1'\right)}.
\end{aligned} \tag{35}$$

The last unknown coefficient $S_4^{(2)}$ can be obtained using the mixed boundary conditions (22) and (23). A function, similar to dislocation density function in mechanical fields, is defined as

$$\Theta\left(z', s\right) = \frac{\partial}{\partial z'}\left[\tilde{T}_2^{(1)\prime}\left(R_1', z', s\right) - \tilde{T}_2^{(2)\prime}\left(R_1', z', s\right)\right]. \tag{36}$$

This gradient function is crucial for obtaining the two-dimensional temperature field caused by the crack with the adoption of the singular integral equation method.

Thus, from Equation (22), one could have

$$\Theta\left(z', s\right) = 0, \quad \left|z'\right| \geq 1, \tag{37}$$

$$\int_{-1}^{1} \Theta\left(z', s\right) dz' = 0, \quad \left|z'\right| < 1. \tag{38}$$

Equation (38), referred as the single-valuedness condition, is obtained from the zero value of temperature jump at the crack tips $|z'| = 1$. It also reflects the fact that the temperature jump starts from zero at $z' = -1$, then increases to a specific value within the crack, and finally decreases to zero again at the other tip $z' = 1$. Substituting Equations (32) and (34) into Equation (36) results in

$$S_4^{(2)} = \frac{1}{j\xi X_6}\int_{-1}^{1} \Theta(\eta, s) e^{-j\xi\eta} d\eta, \tag{39}$$

in which

$$\begin{aligned}
X_6 &- \frac{X_2 X_5}{X_1} I_0\left(\sqrt{k_3^{(1)}} R_1'\right) + X_5 K_0\left(\sqrt{k_3^{(1)}} R_1'\right) \\
&+ \frac{X_4}{X_3} I_0\left(\sqrt{k_3^{(2)}} R_1'\right) - K_0\left(\sqrt{k_3^{(2)}} R_1'\right).
\end{aligned} \tag{40}$$

Substituting Equations (25), (32), (33), (34) and (39) into Equation (23) results in a singular integral equation,

$$\int_{-1}^{1}\Theta(\eta,s)\left[\frac{1}{z'-\eta}+L\left(z',\eta\right)\right]d\eta=\frac{\pi H(s)}{X_\infty},\tag{41}$$

in which

$$L\left(z',\eta\right)=\int_0^\infty\frac{X_9-X_\infty}{X_\infty}\sin\left[\xi\left(z'-\eta\right)\right]d\xi,\tag{42}$$

$$X_9=\left[X_5X_8-\frac{X_2X_5X_7}{X_1}+\frac{X_4}{X_3}I_0\left(\sqrt{k_3^{(2)}}R_1'\right)-K_0\left(\sqrt{k_3^{(2)}}R_1'\right)\right]/\xi X_6,\tag{43}$$

$$X_7=I_0\left(\sqrt{k_3^{(1)}}R_1'\right)-V'k_2^{(1)}\sqrt{k_3^{(1)}}I_1\left(\sqrt{k_3^{(1)}}R_1'\right),\tag{44}$$

$$X_8=K_0\left(\sqrt{k_3^{(1)}}R_1'\right)+V'k_2^{(1)}\sqrt{k_3^{(1)}}K_1\left(\sqrt{k_3^{(1)}}R_1'\right),\tag{45}$$

$$X_\infty=\lim_{\xi\to\infty}X_9=-\frac{V'}{\left(1/k_2^{(1)}\upsilon^{(1)}\right)+\left(1/k_2^{(2)}\upsilon^{(2)}\right)},\tag{46}$$

$$H(s)=V'k_2^{(1)}\sqrt{k_1^{(1)}}\left[S_1^{(1)}I_1\left(\sqrt{k_1^{(1)}}R_1'\right)-S_2^{(1)}K_1\left(\sqrt{k_1^{(1)}}R_1'\right)\right].\tag{47}$$

The singular integral equation (41) under the single-valuedness condition (38) has the fundamental solution [42].

$$\Theta(\eta,s)=f(\eta,s)\left(1-\eta^2\right)^{-1/2}.\tag{48}$$

The Gauss-Jacobi integration formulas in [31] can be adopted to solve Equations (41) and (38) numerically as

$$\sum_{\mu=1}^{N}\frac{1}{N}f\left(\eta_\mu,s\right)\left[\frac{1}{z_\omega'-\eta_\mu}+L\left(z_\omega',\eta_\mu,s\right)\right]=\frac{H(s)}{X_\infty},\tag{49}$$

$$\sum_{\mu=1}^{N}f\left(\eta_\mu,s\right)=0,\tag{50}$$

in which

$$\eta_\mu=\cos\left(\frac{2\mu-1}{2N}\pi\right),\quad \mu=1,2,\cdots,N,\tag{51}$$

$$z_\omega'=\cos\left(\frac{\omega}{N}\pi\right),\quad \omega=1,2,\cdots,N-1.\tag{52}$$

After getting $f(\eta,s)$, the four unknown coefficients in the general solution of P2 given by Equation (2) can be calculated using Equations (34), (39) and (48).

4. Transient Temperature Field and Heat Concentration

Addition of Equation (24) and Equation (2) results in the transient temperature

$$\tilde{T}^{(i)\prime}=\frac{1}{\pi}\int_0^\infty\left[S_3^{(i)}I_0\left(\sqrt{k_3^{(i)}}r'\right)+S_4^{(i)}K_0\left(\sqrt{k_3^{(i)}}r'\right)\right]\cos\left(\xi z'\right)d\xi+S_1^{(i)}I_0\left(\sqrt{k_1^{(i)}}r'\right)+S_2^{(i)}K_0\left(\sqrt{k_1^{(i)}}r'\right),\quad i=1,2,\tag{53}$$

in which, $S_3^{(1)}$, $S_4^{(1)}$, and $S_3^{(2)}$ are expressions of $S_4^{(2)}$. And the Gauss-Chebyshev integration equation can be adopted to numerically calculate $S_4^{(2)}$ from Equation (39),

$$S_4^{(2)}=\frac{-1}{\xi X_6}\int_{-1}^{1}\Theta(\eta,s)\sin(\xi\eta)d\eta=\frac{-1}{\xi X_6}\sum_{\mu=1}^{N}\frac{\pi}{N}f\left(\eta_\mu,s\right)\sin\left(\xi\eta_\mu\right).\tag{54}$$

Similar to the stress intensity factor, heat flux intensity factor (HFIF) is introduced to judge the heat concentration degree around the crack tip quantitatively, as

$$K_q(t)=\lim_{z\to c}\sqrt{2(z-c)}q_r^{(2)}(R_1,z,t).\tag{55}$$

Using the parameter $K_q'=K_q\sqrt{c}/(\lambda_{rr}^{(0)}T_0)$, HFIF can be nondimensionalized in the Laplace domain as

$$\tilde{K'}_q(s)=\lim_{z'\to1}\sqrt{2\left(z'-1\right)}\tilde{q}'^{(2)}_r\left(R_1',z',s\right).\tag{56}$$

Substituting Equations (25) and (33) into Equation (56) leads to

$$\tilde{K'}_q(s)=\prod\lambda_6^{(2)}f(1,s),\tag{57}$$

in which, $f(1,s)$ is calculated from $f(\eta_\mu,s)$ using the interpolation method and

$$\prod=\frac{1}{\left(\lambda_6^{(2)}/\lambda_6^{(1)}\right)\left(1/\upsilon^{(1)}\right)+\left(1/\upsilon^{(2)}\right)}.\tag{58}$$

It can be clearly seen from Equation (58) that the HFIF is dependent on thermal properties of the material on both sides of the crack. Finally, the transient temperature field and HFIF in the time domain can be numerically transformed using the Laplace inversion technique given in [43].

5. Numerical Results

In this section, the solution procedure is verified first. Then, the effects of crack face resistance, liner material, and crack length on the transient temperature field and HFIF of a

Table 1: Thermal properties [46].

Material	ρ (kg/m^3)	c_P (J/kgK)	λ (W/mK)	τ (s)
Carbon	1710	830	190	0.8 [47]
Resin	1200	1050	8	
Steel	7800	490	45	1.6×10^{-12} [48]
Ceramic	3300	670	80	2.7×10^{-6} [49]
Tantalum	16600	139	54.4	1.0×10^{-7} [50]

composite tube containing an interface crack are analyzed in the following three subsections.

The composite tube with initial temperature $T_0 = 300\,\mathrm{K}$ has the size $R_0 = 0.006\,\mathrm{m}$, $R_1 = 0.008\,\mathrm{m}$ and $R_2 = 0.01\,\mathrm{m}$. By assuming the fully conductive inner and outer surfaces as $h_i = h_o = \infty$, the non-Fourier heat conduction of the cracked tube with sudden temperature rise applied on the inner surface $T_a(t) = 330H(t)\,\mathrm{K}$ is investigated based on the C-V model, in which, $H(t)$ is the Heaviside step function. The inner layer can be made of steel, silicon carbide ceramic, or tantalum, while the outer layer is carbon fiber reinforced resin matrix composite. Table 1 lists properties of all the material. It should be mentioned that the accurate value of phase lag of the carbon fiber reinforced composite cannot be found in experimental tests, and it is assumed according to Ref. [41]. Phase lag of heat flux is in the order of picoseconds for most of metals due to the phonon-electron coupling effect. This parameter can be as large as 10^2 s [37] for nonhomogeneous materials, as the thermal flow needs time to circumvent inclusions or pass through the interface of different materials. The experimental evidence of non-Fourier heat conduction in some materials at room temperature can also be found [44, 45].

The macroscopically equivalent material properties of the composite are calculated as [51]

$$\begin{aligned}
\lambda_r^{(2)} &= \lambda_f + \frac{1 - c_1}{1/(\lambda_m - \lambda_f) + c_1/(2\lambda_f)}, \\
\lambda_z^{(2)} &= c_1\lambda_f + (1 - c_1)\lambda_m, \\
c_P^{(2)} &= c_1 c_{Pf} + (1 - c_1)c_{Pm}, \\
\rho^{(2)} &= c_1\rho_f + (1 - c_1)\rho_m,
\end{aligned} \tag{59}$$

in which, the parameters with subscripts "f" and "m," respectively, refer to those of fiber and matrix. Moreover, the fiber fraction c_1 is taken to be 0.2 in this section. The structure profile described here is used in this whole section except Subsection 5.1 designed for validation with reference.

5.1. Validation of the Solution Procedure. Before starting the analysis of the parameters, the solution procedure presented above should be validated. As stated in Introduction, the C-V heat conduction model is accurate to describe the temperature distribution in processed meat and other materials measured by especially designed experiments. However, these kinds of experiment are not available for tubes with or without cracks. The numerical calculation of the transient temperature field for cylindrical cracks using the Fourier or non-Fourier models is also absent among the literature. Thus, the temperature result for uncracked tubes based on the C-V model obtained by Babaei and Chen [52] is adopted for comparison. The same structure, material properties, thermal loading, and nondimensional parameters as those in Ref. [52] for homogeneous tubes are employed, while the cylindrical crack in the present model spreads along the middle plane $R_1{}' = 0.8$ and is assumed insulated. Figure 2 illustrates the nondimensional temperature distribution along the radial direction at the instant $t' = 0.126$ for different axial locations. The Saint-Venant principle indicates that the continuous temperature field at a position far away from the crack will not be affected, which means the same temperature distribution as that in uncracked tubes. This is verified by comparing the temperature distribution at $z' = 10$ for a cracked tube with the results in [52] for an uncracked tube. The dash-dot line depicts the temperature in the cross section across the crack face midpoints. As the crack is insulated, thermal energy will accumulate before the crack and a much higher temperature will then be obtained.

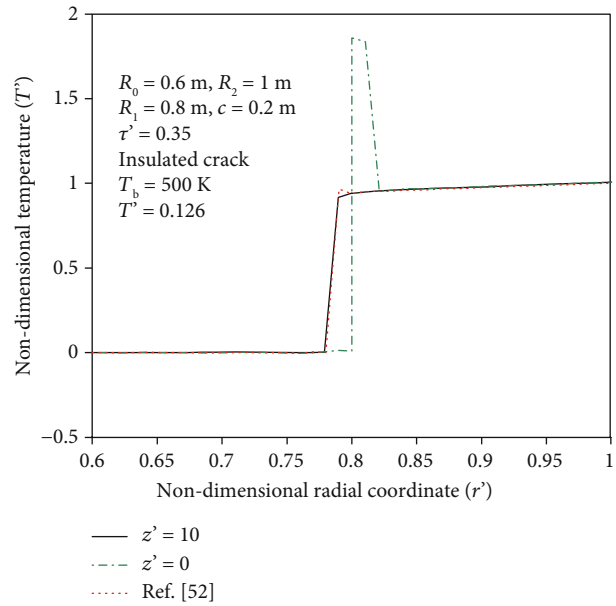

Figure 2: Validation of temperature distribution with Ref. [52].

5.2. The Effect of Thermal Resistance. The effects of crack resistance V on the temperature field and HFIF are shown in Figures 3 and 4, respectively. An infinitely large V corresponding to an insulated crack is compared with three other partially insulated cracks with $V = 1 \times 10^{-3}\,\mathrm{km^2sJ^{-1}}$, $V = 1 \times 10^{-4}\,\mathrm{km^2sJ^{-1}}$, and $V = 1 \times 10^{-5}\,\mathrm{km^2sJ^{-1}}$. The inner layer is made of steel, and a crack with a length of 0.006 m affects the temperature field of the tube remarkably.

Figure 3(a) illustrates the temperature distribution along the interface for different values of V at the instant $t = 3.184$ s when the transient temperature field approaches to the equilibrium state. It is shown that the temperature jump across

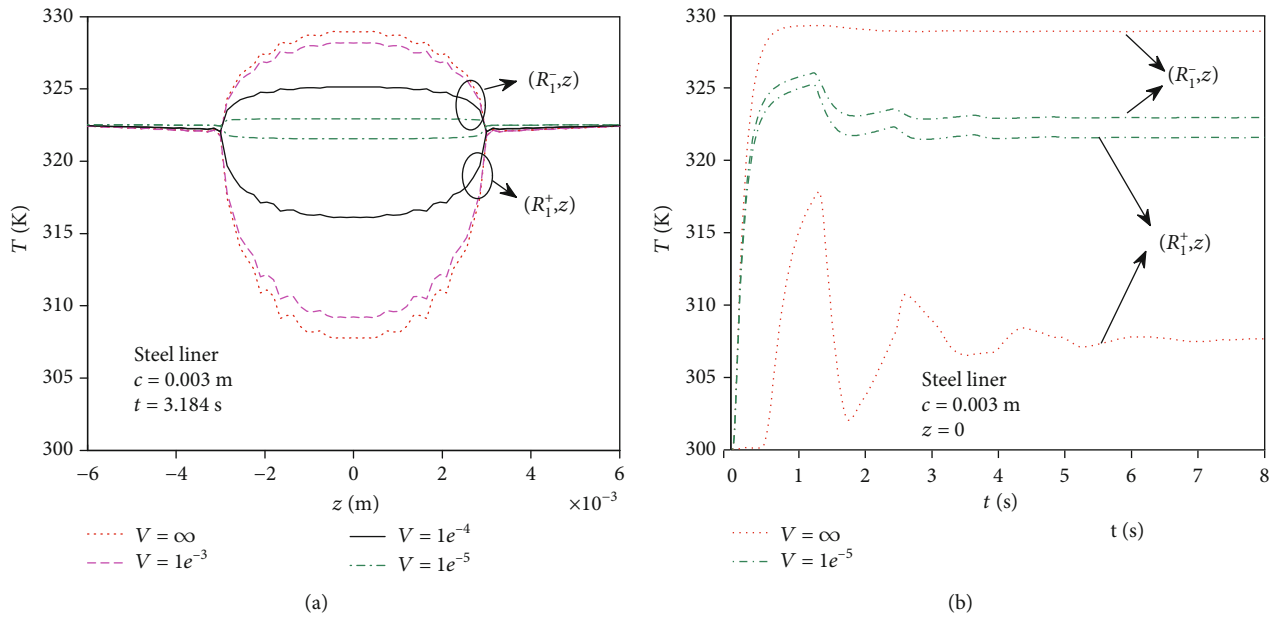

Figure 3: Effect of crack resistance on (a) temperature distribution along the interface plane and (b) temperature history at the crack face midpoints.

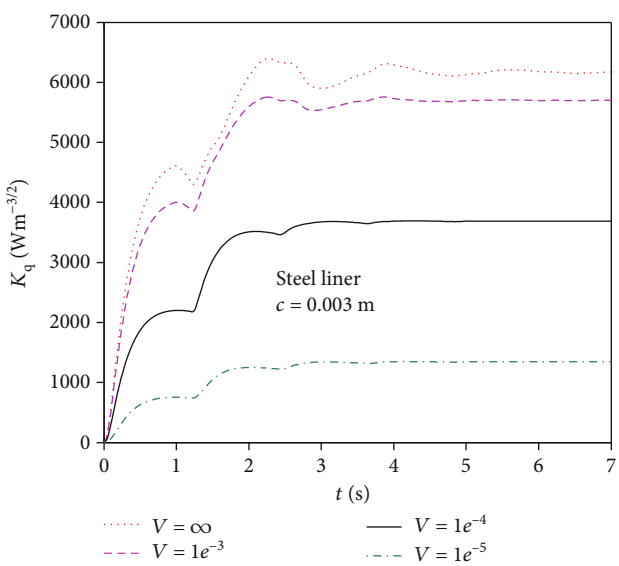

Figure 4: Effect of crack resistance on the HFIF history.

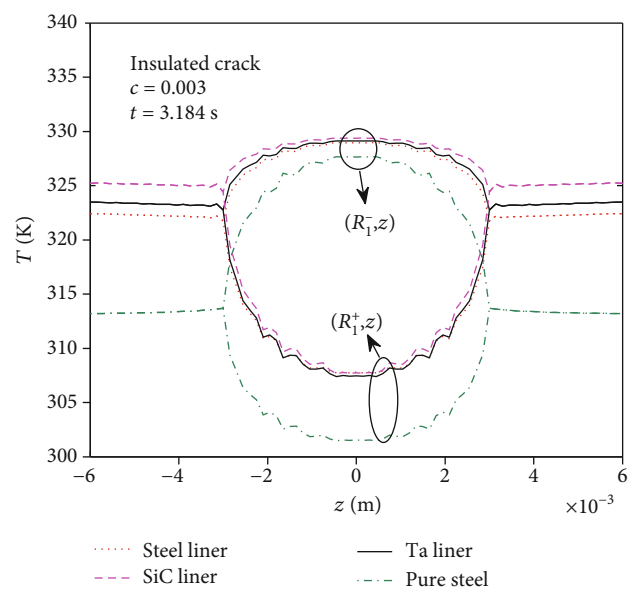

Figure 5: Effect of liner material on the temperature distribution along the interface plane.

the crack face exists for all the cases, while the temperature is continuous along other parts of the interface plane. Also, the temperature at the inner crack face is higher than that in the outer crack face. With the reduction of V, the temperature jump shrinks as well, and the perturbation effect of crack on the temperature fades away. Similar results were reported by Chen and Hu [19] for layered structures as well. Furthermore, the temperature histories at the crack face midpoints for the insulated crack case and almost conducting crack case ($V = 1 \times 10^{-5}\,\mathrm{km^2sJ^{-1}}$) are shown in Figure 3(b). It can be seen that the temperature history performs in an obviously wave-like manner and oscillates around a steady value. Figure 3(b) also depicts the fact that the temperature jump across the insulated crack faces is much higher than that across the conducting crack faces all the while. The oscillating behavior of transient HFIF is shown in Figure 4. Similar to the temperature results, the effect of V on the HFIF indicates that the heat concentration degree reduces with the raise of thermal conduction capability of the crack.

5.3. The Effect of Liner Material. Usage of thermally protective liners is very helpful for the enhancement of the overall performance of composite structure. In this subsection, three kinds of material are chosen to study their effects on thermal behaviors of composite tubes containing an

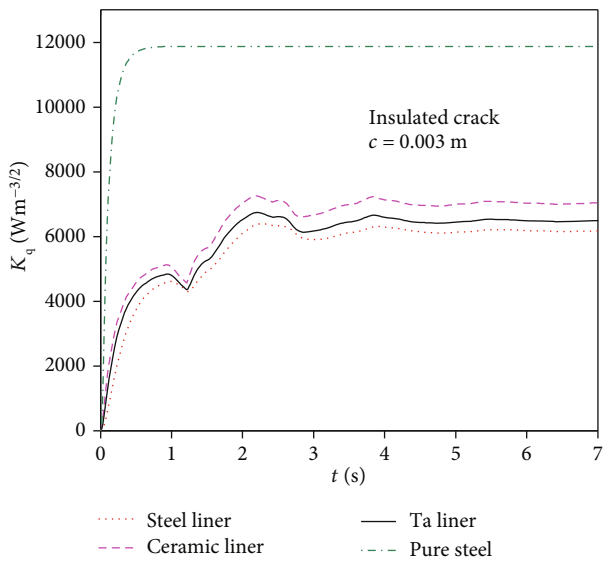

Figure 6: Effect of liner material on the HFIF history.

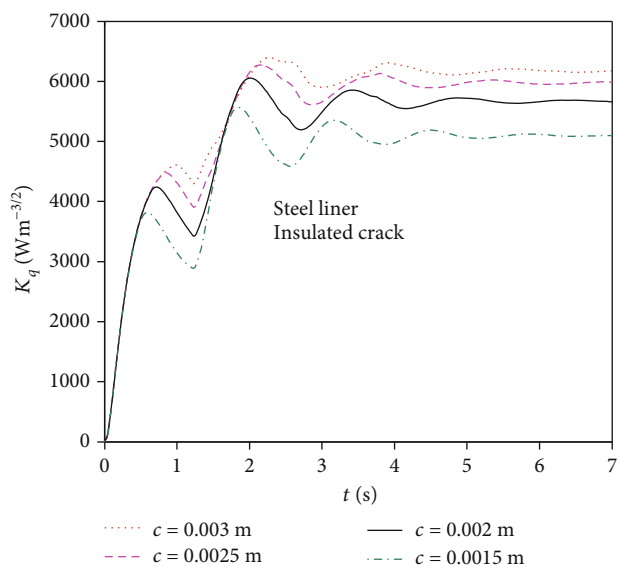

Figure 8: Effect of crack length on the HFIF history.

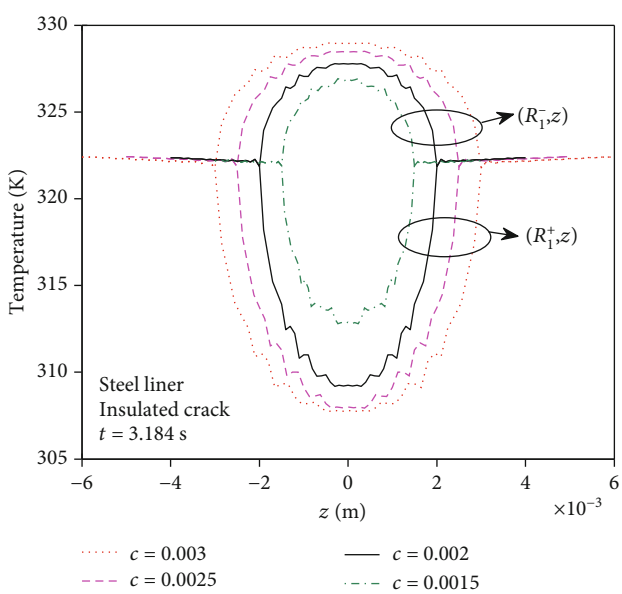

Figure 7: Effect of crack length on the temperature distribution along the interface plane.

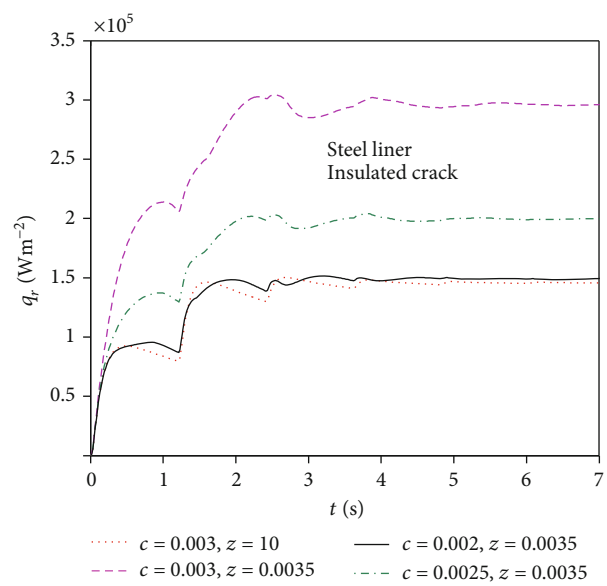

Figure 9: The effect of crack length on the history of heat flux at interface.

insulated interface crack, while a tube with the same size made of pure steel is added for comparison. Please note that the phase lag of steel is so small that the non-Fourier effect is negligible for the steel tube considered in this paper, which has been verified by comparing with the obtained results when setting $\tau = 0$ of steel manually. Thus, the results for steel tube can generally represent thermal behaviors predicted by the Fourier model. And, the crack length is taken to be $c = 0.003$ m.

The temperature distribution along the interface of the four tubes at the instant $t = 3.184$ s is depicted in Figure 5, while Figure 6 shows the HFIF history. Besides the conclusions obtained from Figure 3(a), Figure 5 reveals that the composite tube with steel liner has the lowest temperature off the crack compared with the other two tubes with silicon carbide and tantalum liner. However, their temperatures at the crack midpoints show a negligible difference. Although the temperature of the steel tube is lowest, it has the highest weight as well as heat concentration degree as shown in Figure 6. It can also been observed from Figure 6 that HFIF of the steel tube increases rapidly to the maximum value without oscillating as other tubes. This difference comes from the significant non-Fourier effect of fiber reinforced resin matrix material. The oscillation behavior of the heat flux and HFIF predicted by the non-Fourier models is also described in [20, 53]. Similar

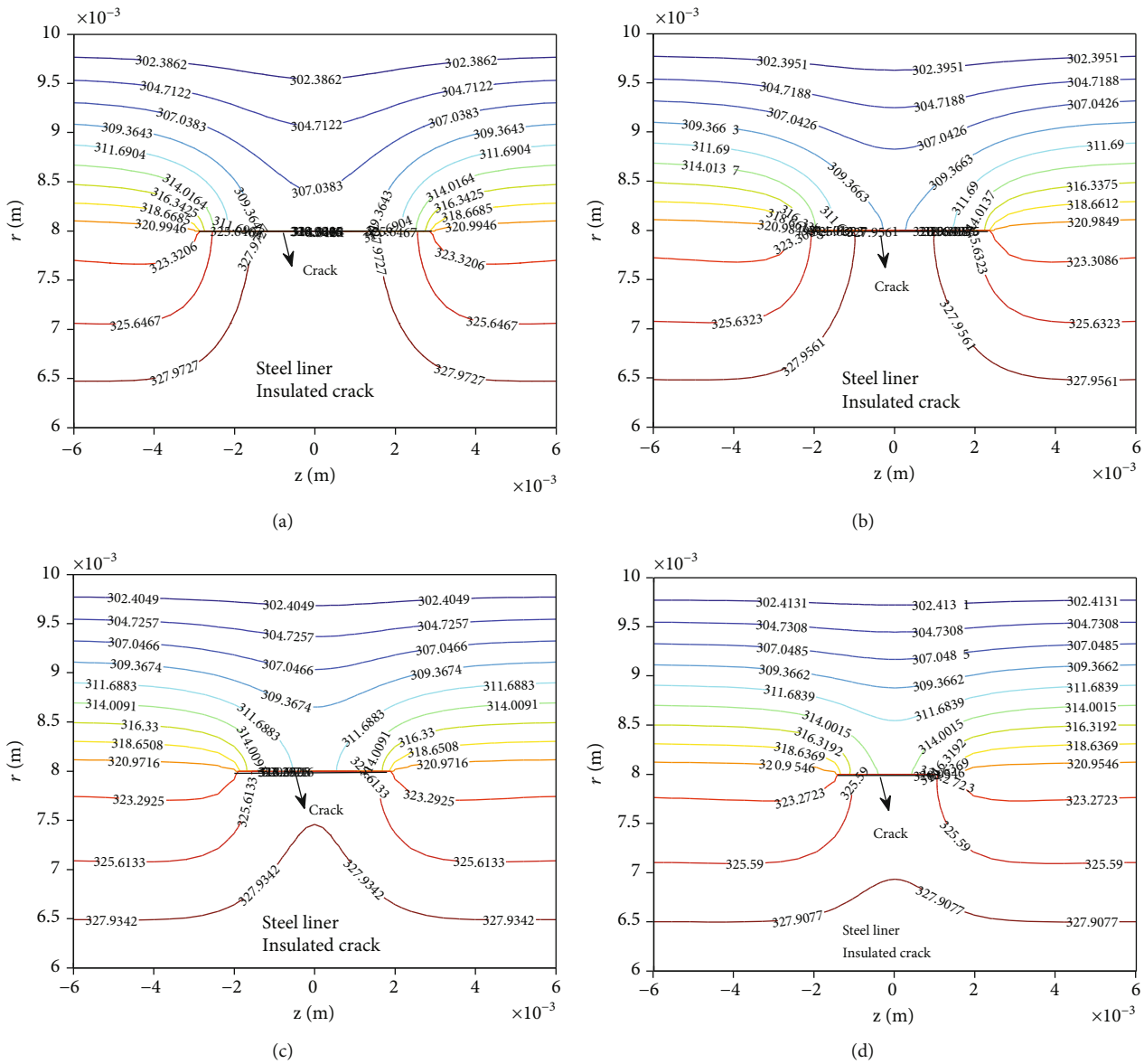

Figure 10: Effect of crack length on the 2D temperature distribution around the crack: (a) $c = 0.003$ m, (b) $c = 0.0025$ m, (c) $c = 0.002$ m, and (d) $c = 0.0015$ m.

to temperature, the tube with steel liner has the lowest HFIF among the three composite tubes.

5.4. The Effect of Crack Length. The effects of crack length on the temperature field, heat flux, and HFIF are described in Figures 7–10. Four composite tubes with steel liner containing different lengths of insulated interface crack, namely, $c = 0.003$ m, 0.0025 m, 0.002 m, and 0.0015 m, are utilized as examples in this subsection. It can be figured out from Figure 7, which shows the temperature distribution along the interface at the instant $t = 3.184$ s, that the shrink of crack length reduces the temperature jump across the crack faces. It can be imagined that the temperature will be continuous across the crack faces when the crack shortens to a size as small as possible. Coincidentally, Figure 8 shows that the HFIF generally reduces as the crack length shrinks.

The histories of heat flux in the radial direction at the same point ($r = 0.008$ m, $z = 0.0035$ m) for different crack lengths are shown in Figure 9, in which the result at the point ($r = 0.008$ m, $z = 10$ m) far away from the crack ($c = 0.003$ m) is incorporated for comparison. The heat flux at the point $z = 10$ m will not be affected by the crack and represents the result for uncracked structure. It is seen that the heat flux from the liner to composite material decreases with the reduction of crack length, as the point picked to plot the result becomes away from the crack tip. The tiny discrepancy between the black line and red line shows that the crack $c = 0.002$ m is too short to affect the heat flux at the point $z = 0.0035$ m.

In order to show the influence of crack on the temperature field more clearly, Figure 10 draws the temperature contour around the crack for different crack lengths at the

instant when the maximum temperature happens. It is clear that heat gathers around the crack tip and temperature jump across the crack faces exists, while the temperature field approaches uniform at positions far away from the crack. Similar to the tendency shown in Figure 7, a shorter crack leads to a more homogeneous temperature field.

6. Conclusion

This paper studies the thermal concentration behavior of a bilayered composite tube containing a cylindrical interface crack. The two-dimensional temperature field disturbed by the crack is obtained using the singular integral equation method. By taking the crack as partially thermal insulated, the effects of crack resistance, liner material, and crack length on the temperature field and HFIF of the cracked tube are analyzed numerically. The following main conclusions are arrived:

(1) Heat flux intensity factor serves as an effective parameter to describe the heat concentration degree caused by the crack quantitatively;

(2) Steel is the best liner material among the three potential materials used for protecting the barrel from the transient temperature change of the inner environment, as the composite tube with steel liner has the lowest temperature and HFIF results compared with the other two liner materials;

(3) The insulating degree of crack affects the heat concentration around the crack tip remarkably. The temperature jump across the crack faces is highest for fully insulated cracks, while the temperature jump and corresponding HFIF decreases when the crack becomes more conductive;

(4) When a small crack grows along the interface, a severer temperature diagram with higher HFIF emerges. This indicates that the crack length in the tube should be controlled to a size as small as possible during the manufacturing process, and the crack detection of the tube in service should be conducted regularly to avoid overheating around the crack tip

Data Availability

The data used to support the findings of this study are included within the article.

Conflicts of Interest

The authors declare that they have no conflicts of interest.

Acknowledgments

This work is supported by the National Natural Science Foundation of China (grant number 11702137), Natural Science Foundation of Jiangsu Province of China (grant number BK20170816), and the Fundamental Research Funds for the Central Universities (grant number 309171B8802).

References

[1] C. Ghita, N. Pop, and I. N. Popescu, "Existence result of an effective stress for an isotropic visco-plastic composite," *Computational Materials Science*, vol. 64, pp. 52–56, 2012.

[2] M. I. A. Othman and I. A. Abbas, "Effect of rotation on plane waves at the free surface of a fibre-reinforced thermoelastic half-space using the finite element method," *Meccanica*, vol. 46, no. 2, pp. 413–421, 2011.

[3] C. Itu, A. Öchsner, S. Vlase, and M. I. Marin, "Improved rigidity of composite circular plates through radial ribs," *Proceedings of the Institution of Mechanical Engineers, Part L: Journal of Materials: Design and Applications*, vol. 233, no. 8, pp. 1585–1593, 2018.

[4] G. C. Sih, "Heat conduction in the infinite medium with lines of discontinuities," *Journal of Heat Transfer*, vol. 87, no. 2, pp. 293–298, 1965.

[5] D. Y. Tzou, "The singular behavior of the temperature gradient in the vicinity of a macrocrack tip," *International Journal of Heat and Mass Transfer*, vol. 33, no. 12, pp. 2625–2630, 1990.

[6] C. Wen-Hwa and C. Chi-Lone, "Heat conduction analysis of a plate with multiple insulated cracks by the finite element alternating method," *International Journal of Solids and Structures*, vol. 31, no. 10, pp. 1343–1355, 1994.

[7] C. K. Chao and R. C. Chang, "Steady-state heat conduction problem of the interface crack between dissimilar anisotropic media," *International Journal of Heat and Mass Transfer*, vol. 36, no. 8, pp. 2021–2026, 1993.

[8] Y. C. Shiah and Y. X. Shi, "Anisotropic heat conduction across an interface crack/defect filled with a thin interstitial medium," *Engineering Analysis with Boundary Elements*, vol. 30, no. 5, pp. 325–337, 2006.

[9] T. C. Chiu, S. W. Tsai, and C. H. Chue, "Heat conduction in a functionally graded medium with an arbitrarily oriented crack," *International Journal of Heat and Mass Transfer*, vol. 67, pp. 514–522, 2013.

[10] Y. Zhou, X. Li, and D. Yu, "A partially insulated interface crack between a graded orthotropic coating and a homogeneous orthotropic substrate under heat flux supply," *International Journal of Solids and Structures*, vol. 47, no. 6, pp. 768–778, 2010.

[11] C. F. Gao and N. Noda, "Thermal-induced interfacial cracking of magnetoelectroelastic materials," *International Journal of Engineering Science*, vol. 42, no. 13-14, pp. 1347–1360, 2004.

[12] J. Wang, Z. H. Jin, and C. F. Gao, "A mode II cohesive crack in an infinite medium subjected to remote heat flux – effect of thermal resistance of the cohesive zone," *Engineering Fracture Mechanics*, vol. 204, pp. 147–156, 2018.

[13] C. Cattaneo, "A form of heat conduction equation which eliminates the paradox of instantaneous propagation," *Comptes Rendus*, vol. 247, no. 4, pp. 431–433, 1958.

[14] P. Vernotte, "Some possible complications in the phenomena of thermal conduction," *Compte Rendus*, vol. 252, pp. 2190-2191, 1961.

[15] K. Mitra, S. Kumar, A. Vedevarz, and M. K. Moallemi, "Experimental evidence of hyperbolic heat conduction in processed meat," *Journal of Heat Transfer*, vol. 117, no. 3, pp. 568–573, 1995.

[16] W. Kaminski, "Hyperbolic heat conduction equation for materials with a nonhomogeneous inner structure," *Journal of Heat Transfer*, vol. 112, no. 3, pp. 555–560, 1990.

[17] J. W. Fu, Z. T. Chen, and L. F. Qian, "Coupled thermoelastic analysis of a multi-layered hollow cylinder based on the C–T theory and its application on functionally graded materials," *Composite Structures*, vol. 131, pp. 139–150, 2015.

[18] I. A. Abbas and M. Marin, "Analytical solution of thermoelastic interaction in a half-space by pulsed laser heating," *Physica E: Low-dimensional Systems and Nanostructures*, vol. 87, pp. 254–260, 2017.

[19] Z. T. Chen and K. Q. Hu, "Hyperbolic heat conduction in a cracked thermoelastic half-plane bonded to a coating," *International Journal of Thermophysics*, vol. 33, no. 5, pp. 895–912, 2012.

[20] K. Q. Hu and Z. T. Chen, "Transient heat conduction analysis of a cracked half-plane using dual-phase-lag theory," *International Journal of Heat and Mass Transfer*, vol. 62, pp. 445–451, 2013.

[21] W. Li, J. Li, R. Abdelmoula, F. Song, and C. P. Jiang, "Inertia effect analysis of a half-plane with an induced crack under thermal loading using hyperbolic heat conduction," *ZAMM - Journal of Applied Mathematics and Mechanics / Zeitschrift für Angewandte Mathematik und Mechanik*, vol. 96, no. 8, pp. 939–955, 2016.

[22] W. Li, F. Song, J. Li, R. Abdelmoula, and C. Jiang, "Non-Fourier effect and inertia effect analysis of a strip with an induced crack under thermal shock loading," *Engineering Fracture Mechanics*, vol. 162, pp. 309–323, 2016.

[23] Z. N. Xue, Z. T. Chen, and X. G. Tian, "Thermoelastic analysis of a cracked strip under thermal impact based on memory-dependent heat conduction model," *Engineering Fracture Mechanics*, vol. 200, pp. 479–498, 2018.

[24] J. W. Fu, A. H. Akbarzadeh, Z. T. Chen, L. F. Qian, and D. Pasini, "Non-Fourier heat conduction in a sandwich panel with a cracked foam core," *International Journal of Thermal Sciences*, vol. 102, pp. 263–273, 2016.

[25] M. Marin, S. Vlase, and M. Paun, "Considerations on double porosity structure for micropolar bodies," *AIP Advances*, vol. 5, no. 3, 2015.

[26] M. Marin, E. M. Craciun, and N. Pop, "Considerations on mixed initial-boundary value problems for micropolar porous bodies," *Dynamic Systems and Applications*, vol. 25, pp. 175–196, 2016.

[27] M. Marin, R. P. Agarwal, and D. Baleanu, "On a generalized relaxed saint–Venant principle," *Boundary Value Problems*, vol. 2018, no. 1, 2018.

[28] S. L. Guo, B. L. Wang, and C. Zhang, "Thermal shock fracture mechanics of a cracked solid based on the dual-phase-lag heat conduction theory considering inertia effect," *Theoretical and Applied Fracture Mechanics*, vol. 86, pp. 309–316, 2016.

[29] X. Y. Zhang, Z. T. Chen, and X. F. Li, "Thermal shock fracture of an elastic half-space with a subsurface penny-shaped crack via fractional thermoelasticity," *Acta Mechanica*, vol. 229, no. 12, pp. 4875–4893, 2018.

[30] J. Fu, Z. Chen, L. Qian, and K. Hu, "Transient thermoelastic analysis of a solid cylinder containing a circumferential crack using the C-V heat conduction model," *Journal of Thermal Stresses*, vol. 37, no. 11, pp. 1324–1345, 2014.

[31] J. Fu, Z. Chen, L. Qian, and Y. Xu, "Non-Fourier thermoelastic behavior of a hollow cylinder with an embedded or edge circumferential crack," *Engineering Fracture Mechanics*, vol. 128, pp. 103–120, 2014.

[32] J. W. Fu, Z. T. Chen, L. F. Qian, and Y. D. Xu, "Thermal fracture of cracked cylinders associated with nonclassical heat conduction: the effect of material property," *Journal of Thermal Stresses*, vol. 39, no. 9, pp. 1119–1137, 2016.

[33] X. Y. Zhang and X. F. Li, "Transient thermal stress intensity factors for a circumferential crack in a hollow cylinder based on generalized fractional heat conduction," *International Journal of Thermal Sciences*, vol. 121, pp. 336–347, 2017.

[34] Z. N. Xue, Z. T. Chen, and X. G. Tian, "Transient thermal stress analysis for a circumferentially cracked hollow cylinder based on memory-dependent heat conduction model," *Theoretical and Applied Fracture Mechanics*, vol. 96, pp. 123–133, 2018.

[35] W. J. Feng, R. K. L. Su, and Z. Q. Jiang, "Torsional impact response of a cylindrical interface crack between a functionally graded interlayer and a homogeneous cylinder," *Composite Structures*, vol. 68, no. 2, pp. 203–209, 2005.

[36] S. Itou, "Stress intensity factors for a moving cylindrical crack in a nonhomogeneous cylindrical layer in composite materials," *Archive of Applied Mechanics*, vol. 75, no. 1, pp. 18–30, 2005.

[37] Y. D. Li, H. Zhao, and T. Xiong, "The cylindrical interface crack in a layered tubular composite of finite thickness under torsion," *European Journal of Mechanics a-Solids*, vol. 39, pp. 113–119, 2013.

[38] M. Noroozi, A. Atrian, A. Ghassemi, and M. Vahabi, "Torsion analysis of infinite hollow cylinders of functionally graded materials weakened by multiple axisymmetric cracks," *Theoretical and Applied Fracture Mechanics*, vol. 96, pp. 811–819, 2018.

[39] M. Noroozi, A. Ghassemi, A. Atrian, and M. Vahabi, "Multiple cylindrical interface cracks in FGM coated cylinders under torsional transient loading," *Theoretical and Applied Fracture Mechanics*, vol. 97, pp. 258–264, 2018.

[40] S. Itou, "Thermal stresses in an infinite elastic pipe weakened by two cylindrical cracks," *Journal of Thermal Stresses*, vol. 30, no. 11, pp. 1069–1097, 2007.

[41] J. Fu, K. Hu, L. Qian, and Z. Chen, "Non-Fourier heat conduction of a functionally graded cylinder containing a cylindrical crack," *Advances in Mathematical Physics*, vol. 2020, Article ID 8121295, 11 pages, 2020.

[42] F. Erdogan, G. D. Gupta, and T. S. Cook, "Numerical solution of singular integral equations," in *Mechanics of Fracture, Volume 1: Methods of Analysis and Solutions of Crack Problems*, G. C. Sih, Ed., pp. 368–425, Noordhoff, Leyden, Netherlands, 1973.

[43] F. Durbin, "Numerical inversion of Laplace transforms: an efficient improvement to Dubner and Abate's method," *The Computer Journal*, vol. 17, no. 4, pp. 371–376, 1974.

[44] S. Both, B. Czél, T. Fülöp et al., "Deviation from the Fourier law in room-temperature heat pulse experiments," *Journal of Non-Equilibrium Thermodynamics*, vol. 41, no. 1, pp. 41–48, 2016.

[45] P. Van, B. Czel, T. Fulop, G. Grof, A. Gyenis, and J. Verhas, "Experimental aspects of heat conduction beyond Fourier," in *12th Joint European Thermodynamics Conference*, Brescia, Italy, 2013.

[46] W. D. Callister, *Materials Science and Engineering: An Introduction*, John Wiley & Sons, New York, 7th edition, 2007.

[47] L. Zhou, J. Lin, H. Lin, and G. Chen, "Electrical-thermal switching effect in high-density polyethylene/graphite

nanosheets conducting composites," *Journal of Materials Science*, vol. 43, no. 14, pp. 4886–4891, 2008.

[48] P. Francis, "Thermo-mechanical effects in elastic wave propagation: a survey," *Journal of Sound and Vibration*, vol. 21, no. 2, pp. 181–192, 1972.

[49] D. Y. Tzou, *Macro- to Microscale Heat Transfer: The Lagging Behavior*, John Wiley & Sons, UK, 2nd edition, 2015.

[50] A. Vedavarz, S. Kumar, and M. K. Moallemi, "Significance of non-Fourier heat waves in conduction," *Journal of Heat Transfer*, vol. 116, no. 1, pp. 221–224, 1994.

[51] B. W. Rosen and Z. Hashin, "Effective thermal expansion coefficients and specific heats of composite materials," *International Journal of Engineering Science*, vol. 8, no. 2, pp. 157–173, 1970.

[52] M. H. Babaei and Z. Chen, "Transient hyperbolic heat conduction in a functionally graded hollow cylinder," *Journal of Thermophysics and Heat Transfer*, vol. 24, no. 2, pp. 325–330, 2010.

[53] A. H. Akbarzadeh and Z. T. Chen, "Heat conduction in one-dimensional functionally graded media based on the dual-phase-lag theory," *Proceedings of the Institution of Mechanical Engineers, Part C: Journal of Mechanical Engineering Science*, vol. 227, no. 4, pp. 744–759, 2012.